A Bipedal DNA Brownian Motor with Coordinated Legs

Tosan Omabegho, *et al.*

Science **324**, 67 (2009);
DOI: 10.1126/science.1170336

Science (print ISSN 0036-8075; online ISSN 1095-9203) is published weekly, except the last week in December, by the American Association for the Advancement of Science, 1200 New York Avenue NW, Washington, DC 20005.

A Bipedal DNA Brownian Motor with Coordinated Legs

Tosan Omabegho,[1] Ruojie Sha,[2] Nadrian C. Seeman[2]*

A substantial challenge in engineering molecular motors is designing mechanisms to coordinate the motion between multiple domains of the motor so as to bias random thermal motion. For bipedal motors, this challenge takes the form of coordinating the movement of the biped's legs so that they can move in a synchronized fashion. To address this problem, we have constructed an autonomous DNA bipedal walker that coordinates the action of its two legs by cyclically catalyzing the hybridization of metastable DNA fuel strands. This process leads to a chemically ratcheted walk along a directionally polar DNA track. By covalently cross-linking aliquots of the walker to its track in successive walking states, we demonstrate that this Brownian motor can complete a full walking cycle on a track whose length could be extended for longer walks. We believe that this study helps to uncover principles behind the design of unidirectional devices that can function without intervention. This device should be able to fulfill roles that entail the performance of useful mechanical work on the nanometer scale.

Biological bipedal motors, such as kinesin (*1*), myosin (*2*), and dynein (*3*), are all examples of coordinated activity between two motor domains that lead to processive linear movement along directionally polar tracks. How such directed motion emerges from domain coordination is a major issue in the effort to create synthetic molecular motors that can cyclically bias Brownian motion by using chemical energy as input (*4*, *5*). Synthetic DNA walking devices (*6*–*11*) are useful systems to explore these questions because of DNA's programmability and structural robustness. A benchmark goal is the design and construction of controlled autonomous translocators, for example to use in synthetic molecular assembly procedures that emulate nucleic acid polymerases or the ribosome.

It was recently shown in an autonomous DNA bipedal system (*10*) that when the legs of the biped do not communicate, the motion of the biped is random, and it does not remain bound to its track. The implication from such a study and natural systems like kinesin is that coordinated motion is fundamental to the operation of molecular motors. Hence, coordination mechanisms that allow for information feedback between the domains of a device need to be devised.

We present an autonomous bipedal walker made of DNA that walks along a directionally polar DNA track. This device displays true motor behavior by coordinating the stepping cycle of its two legs as it walks along its track; it does this by having its leading leg catalyze the release of its trailing leg. The release signal, sent from the leading leg to the trailing leg, is mediated by metastable DNA fuel strand complexes (*10*–*13*) and aided by the structural asymmetry of the track. Green *et al*. recently showed how the back leg of a DNA biped could be biased for forward movement by its leading leg on a single-stranded DNA substrate that lacks a robust structure (*11*). They outline a clever leg coordination design that may in principle be capable of directed motion on a reusable track. In our experiments, we demonstrated the operation of a biped that completes a fully coordinated unidirectional stepping cycle on a linear stiff track, thereby exhibiting autonomous and directed molecular motion on a track that is consumed.

Our system is made up of 21 DNA strands. As Fig. 1A shows, the walker is a single strand of DNA containing a 5′,5′ linkage in the middle; one leg is called Leg-Even (L-E), and the other is called Leg-Odd (L-O). The walker walks upon a linear double-crossover (DX) (*14*) track, which is designed to be approximately 49 nm long and has a persistence length of ~100 nm (*15*). The track is assembled from 18 strands, four of which are metastable stem-loop structures (T1, T2, T3, and T4) that function both in the operation of the device and as structural elements in the track [supporting online material (SOM) text and fig. S1]. Two metastable hairpin fuel strands, F1 and F2, float freely in solution. To distinguish them from the stationary track stem loops, we refer to the freely floating fuel strands as hairpins.

All the reactions are designed around six "toehold" (*16*) sequences on the loop regions of the track stem loops (Fig. 1, A and B) (see SOM text for a discussion of the sequence design). There is leg-holding site d, a toehold-binding site for L-O on T1 and T3, and leg-holding site a, another toehold-binding site for L-E on both T2 and T4. There are fuel-grabbing sites c and f, which are toeholds for the activation of fuel strands F1 and F2. Fuel-grabbing site c is on T2 and T4, whereas fuel-grabbing site f is on T1 and T3. Finally, there are leg-releasing sites e and b; these are toeholds for the activated fuel molecules F1 and F2 that release walker legs L-O and L-E, respectively.

By controlling these toehold interactions kinetically, we show that the walker can take two steps autonomously from what we call resting-state 1 (RS-1) (Fig. 1C, left) to RS-3 with the simultaneous addition of fuel strands F1 and F2 (Fig. 1C, middle). We also show the one-step intermediate transition from RS-1 to RS-2 when only F1 is added (Fig. 1C, top). To demonstrate control of the system and its dependence on both fuel strands, we show that when F2 alone is added (Fig. 1C, bottom) no transition takes place and that only when F1 is further added does the walker make the transition from RS-1 to RS-3 (Fig. 1C, right). In the experimental demonstrations of the three transitions described above, the system was closed; this was achieved by changing both fuel-grabbing site f on T1 and fuel-grabbing site c on T4 to tracts containing only polythymidine, thereby rendering them both nonspecific and inactive. We also show that when the sequence of fuel-grabbing site c on T4 is restored, the walker transitions to RS-4, incorporating one more F1 molecule into the track (Fig. 1D).

Figure 2 depicts the biped's autonomous transition from RS-1 to RS-2 in 8 sequential steps. Steps 1 to 5 depict the release of L-O from T1 with the incorporation of F1 into the track. The fuel strand that releases the walker biases or rectifies the walker's forward movement by creating a more stable duplex with the stem loop that was holding the released leg (step 5). The catalyzed release of the trailing leg by the leading leg begins in step 6: The leading leg (L-O) first diffuses to and activates its target stem loop (T3) (step 7); as is shown taking place for F1 in steps 1 and 5, F2 then releases L-E from T2, and the walker transitions to RS-3 to complete the cycle (the complete sequence of steps is shown in fig. S3). Step 3 demonstrates how the activated fuel strands have limited single-stranded flexibility (*17*, *18*) and are placed three times closer (7 nm versus 21 nm) to their complementary stem loops (holding the trailing leg of the walker) than to the stem loops one site ahead. This difference in distance, 7 nm versus 21 nm, gives rise to the track's directional polarity. The two metastable topologies the walker forms with the track, when either one or two legs are attached, protect the leg-releasing sequences directly beneath each leg from being accessed by their fuel strands prematurely (SOM text and fig. S4). After one step of the walker, an overall free energy gain corresponding to 20 base pairs (bp) occurs with the incorporation of one fuel molecule into the track: 8 bp for the fuel-grabbing region and 12 bp for the leg-holding and leg-releasing region.

We tracked the progress of the walker by covalently cross-linking aliquots of it to the track as fuel was added and then visualizing the constituent strands of the products in autoradiograms produced from either super-denaturing (*19*) or nondenaturing polyacrylamide gel electrophoresis (PAGE). Each track stem loop was synthesized with a psoralen molecule on its 3′ end; consequently, the track stem loops cross-link across their duplexes when the system is exposed to ultraviolet (UV) light (Fig. 3A) (*1*, *20*). Five experiments were run in parallel: W*; T1*; T2*;

[1]School of Engineering and Applied Sciences, Harvard University, Cambridge, MA 02138, USA. [2]Department of Chemistry, New York University, New York, NY 10003, USA.

*To whom correspondence should be addressed. E-mail: ned.seeman@nyu.edu

T3*; and T4*. In each experiment, only one of the strands was radioactively labeled: W*, walker; T1*, track stem loop T1; T2*, track stem loop T2; T3*, track stem loop T3; and T4*, track stem loop T4. Figure 3B shows the cross-linking reactions that take place in the four resting states (RS-1, RS-2, RS-3, and RS-4) of the track and for each resting state, the experiments in which the walker/stem loop cross-linked products are visible.

The products of the walker cross-linked to the track stem loops will appear as two higher molecular weight bands on super-denaturing PAGE (*21*). A molecule migrates on a denaturing gel as a function of both its size and its topology (*22*). The upper band consists of the walker cross-linked to two stem loops, one on its trailing leg and one on its leading leg [walker–trailing leg–leading leg (w-t-l) product] (Fig. 3C). The lower band contains the walker cross-linked to one stem loop, either on its trailing or on its leading leg (w-t and w-l products, respectively) (Fig. 3C). The formation and global state changes of the track are visible in nondenaturing gels, and the position of the walker on the track is visible in super-denaturing gels.

After an initial annealing step in which the two halves of the track (Fig. 4A, lanes 1 to 5) were combined to assemble the whole track (SOM text and figs. S6 and S7), all five radioactive track species (W*, T1*, T2*, T3*, and T4*) colocalized on a gel to form one band (Fig. 4A, lanes 6 to 10). To show that the assembled track was consistent with state RS-1, we exposed aliquots of all five track solutions to 366 nm of light, capturing the position of the walker. A super-denaturing gel of these five mixtures shows the walker cross-linked almost entirely to T1 and T2 (Fig. 4B, lanes 1 to 5). Pictured on the left hand side of the gel, the resulting cross-linked products are w-t-l (W-T1-T2) in experiments W* (lane 1), T1* (lane 2), and T2* (lane 3); w-t (W-T1) in experiments W* and T1*; and w-l (W-T2) in experiments W* and T2*. [For an explanation of the secondary products seen in the middle of the gel, see SOM text and figs. S8 to S11]

To show that the walker transitioned from RS-1 to RS-2 with the addition of F1, we added F1 to aliquots of all five assembled track solutions. After 1 hour (*23*), the walker clearly transitioned and cross-linked to T2 and T3 (Fig. 4B, lanes 6 to 10). It is clear that both w-t-l (W-T1-T2) and w-t (W-T1) were greatly reduced in experiment T1* (compare lanes 2 and 7), and w-t-l (W-T2-T3) and w-l (W-T3) appeared in experiment T3* (compare lanes 4 and 9), which is consistent with the transition from RS-1 to RS-2. The target products W-T2-T3, W-T2, and W-T3 are pictured on the right of the gel.

To show that the walker took two steps autonomously from RS-1 to RS-3 upon the addition of F1 and F2, we added both fuel strands simultaneously. After 1 hour, a majority of the walker cross-linked to T3 and T4, which is consistent with the transition to RS-3 (Fig. 4C, lanes 6 to 10). As a control, we let aliquots of the track sit without fuel for the same hour: In this experiment, the walker remained on T1 and T2 (lanes 1 to 5), demonstrating that on the time scale of an hour it was the addition of fuel that drove the movement of the walker, and not random diffusion. Quantitation of band intensities established the stepping efficiency of the walker to be 74% for each step of the walker (SOM text, fig. S13, and table S1).

As the walker moved and the track picked up fuel molecules, the molecular weight of the walker and track increased, and its three-dimensional shape changed; as a result, its mobility decreased. These changes can be seen as mobility shifts in a nondenaturing gel (Fig. 4D). In lane 1, an aliquot of experiment W* in state RS-1 acts as a marker. When F1 alone was added, a gel shift occurred reflecting the incorporation of one fuel molecule during the transformation to RS-2 (lanes 2 to 6). When both fuel molecules were added, a larger gel shift was observed, reflecting the incorporation of two fuel molecules during the transformation to RS-3 (lanes 7 to 11). Uniform behavior is seen in all five experiments. Neither free walker nor track multimers are visible in Fig. 4D; this finding strongly suggests that the walkers began and

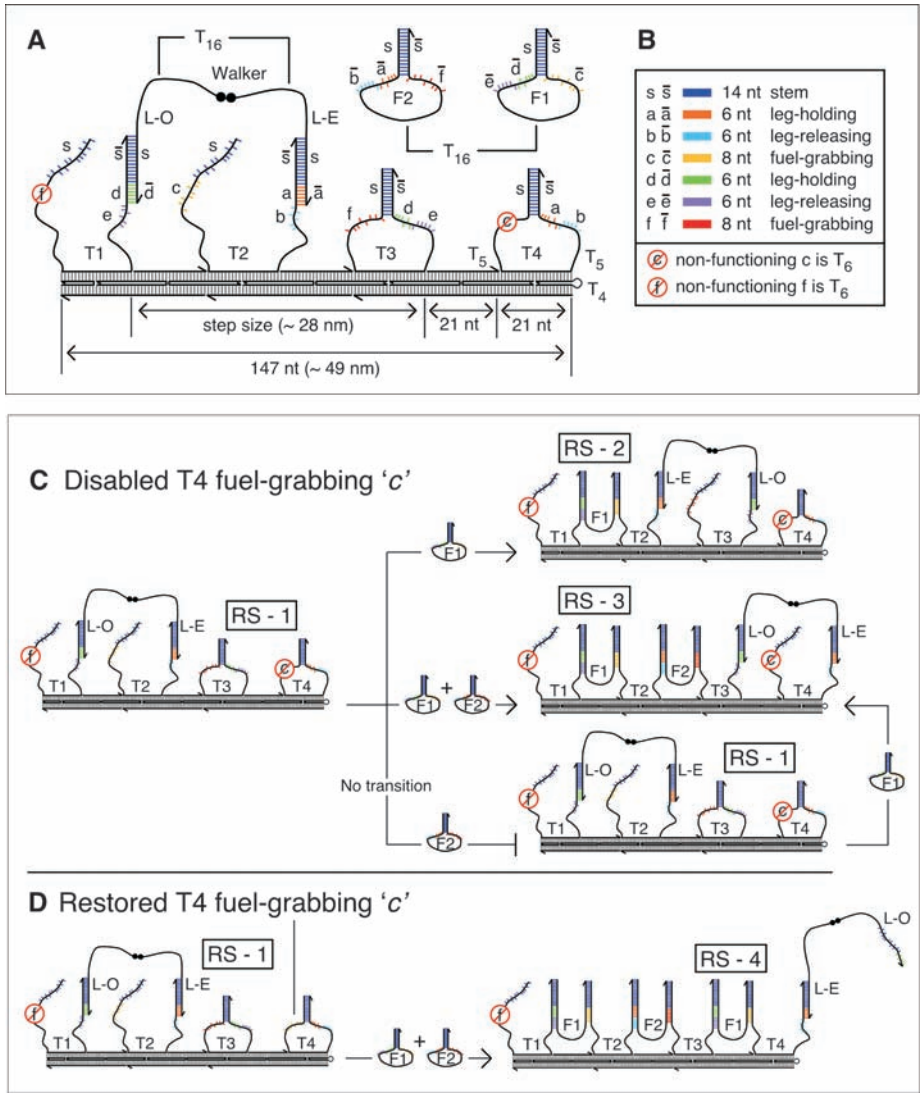

Fig. 1. (**A**) Illustration of the DX track structure with the walker on it. The walker is shown on stem loops T1 and T2. The walker's 5′,5′ linkage is denoted by two black dots and its 3′ ends by half arrows. T_{16} denotes flexible polythymidine linkers on the walker and two fuel hairpins, F1 and F2. Two T_5 regions provide flexibility at the base of the track stem loops. All the binding sites are labeled with lowercase letters, and complementary sequences are capped with a bar. The two fuel-grabbing sequences f and c on T1 and T4, respectively, are not functional. (**B**) Color-coding and the names of the binding sites. (**C**) Transitions made with a nonfunctional T4 fuel-grabbing sequence c. The walker is programmed to take two steps from RS-1 to RS-3 with the addition of F1 and F2 simultaneously (middle). A single step is made from RS-1 to RS-2 with the addition of F1 alone (top). With the addition of F2 alone, the walker does not move, and only with the further addition of F1 does the walker make the transition from RS-1 to RS-3 (bottom). (**D**) With the T4 fuel-grabbing sequence c restored, the walker transitions to RS-4, incorporating another F1 into the track, thereby kicking L-O off of T3.

ended their walks on the same track and coupled their legs by intramolecular interactions.

Further demonstrating control of the system, we added F2 alone to the track for 1 hour and found that the walker primarily remained on and cross-linked to T1 and T2 (Fig. 4E, lanes 1 to 5). When we added F1 to this solution containing the track and F2 and left it to react for another hour, the walker was found cross-linked to T3 and T4 (lanes 6 to 10), again demonstrating that it transitioned from the RS-1 structure to the RS-3 structure only when both fuel molecules were present. A nondenaturing gel (Fig. 4F) also shows that the track that sat in solution with F2 (lanes 2 to 6) colocalized with the track to which no fuel was added (lane 1) and then shifted after F1 was added to this mixture (lanes 7 to 11).

The transition to RS-4 is shown in Fig. 4, G and H. The data in this case indicate that the walker cross-linked primarily to T4 upon the addition of F1 and F2 or that the distribution of product shifted to the w-l product (Fig. 4G, lanes 6 to 10). Figure 4H shows uniform transitioning in the native state. This result further verifies that the system works as designed and that the fuel-grabbing sequences can control the walker's progress.

We have demonstrated the activity of a DNA molecular motor that uses leg coordination to achieve directed bipedal motion in a "burnt bridges" Brownian ratchet–type (*24*, *25*) mechanism whereby the stem loops on the track are consumed irreversibly during the walk. Our work suggests, as does nature, that to cycle a motor along a predefined trajectory and to break directional symmetry, coordination between at least two parts of the motor may be required. Molecular spiders (*8*, *9*) and the recently demonstrated stochastic walker (*10*) are also synthetic autonomous walking systems in which the track is consumed, but they function without leg-coordination mechanisms. In these systems, directional polarity is not built into the system but is strictly imposed

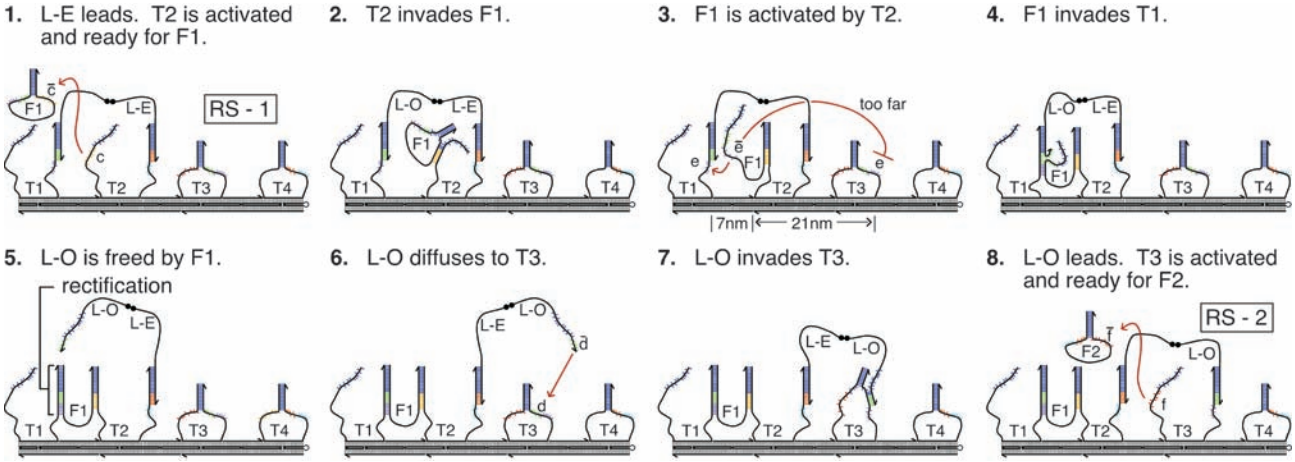

Fig. 2. Transition from RS-1 to RS-2. In eight sequential frames, this illustration depicts the biped taking one step. Illustrations 1 to 5 depict the activation of F1 by T2 and the release of L-O from T1 by F1. The freed leg L-O then begins the catalyzed release of L-E from T2 (illustrations 6 to 8). Key to directionally biasing the biped, illustration 3 shows how the activated fuel strands are spatially restricted to act on the stem loop 7 nm away rather than the stem loop 21 nm away. (The complete transition to RS-3 is shown in fig. S3.)

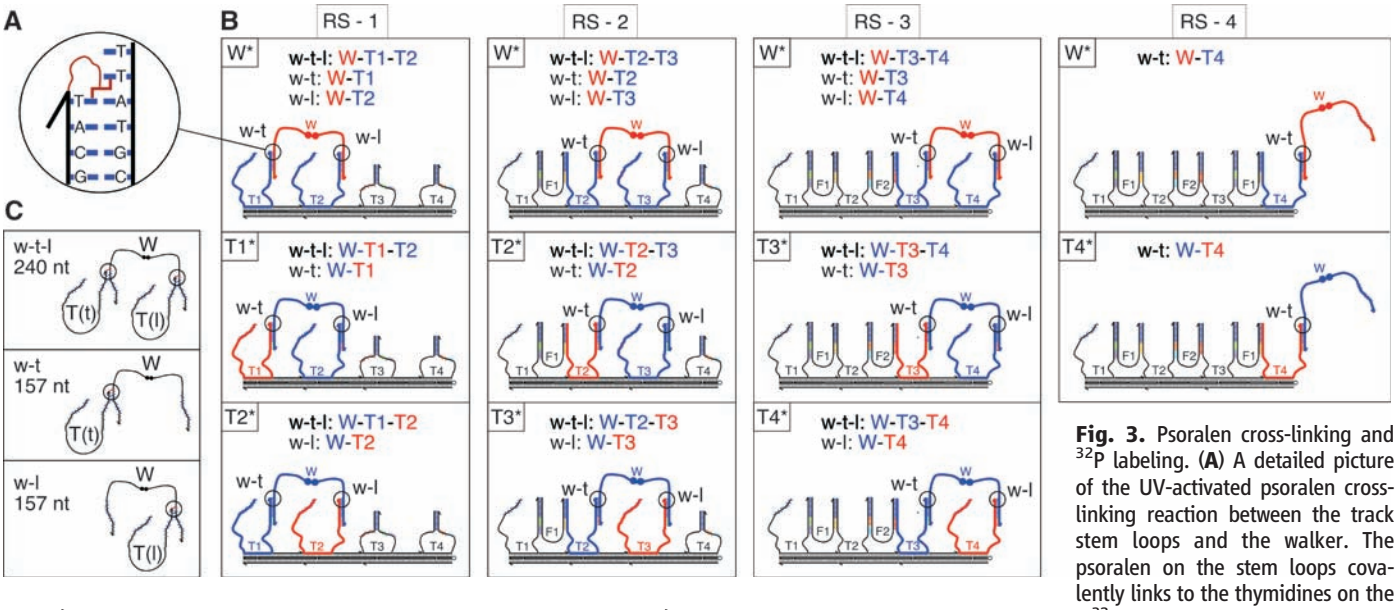

Fig. 3. Psoralen cross-linking and ^{32}P labeling. (**A**) A detailed picture of the UV-activated psoralen cross-linking reaction between the track stem loops and the walker. The psoralen on the stem loops covalently links to the thymidines on the walker's legs just outside the duplex formed by the stem loops and the walker's legs. (**B**) Visualizing the cross-link products with ^{32}P. The three cross-linked products w-t (walker linked to the stem-loop on its trailing leg), w-l (walker linked to the stem-loop on its leading leg), and w-t-l (walker linked on both its trailing and leading leg) are shown forming in each experiment (W*, T1*, T2*, T3*, and T4*) that they are visible for each resting state (RS-1, RS-2, RS-3, and RS-4) of the system. The radioactive strand is drawn in red and the nonradioactive strands that are part of the cross-linked complex are drawn in blue. The constituent components of the products formed are listed in each box. (**C**) Denatured topologies and size of the three walker–stem-loop cross-link products w-t, w-l, and w-t-l.

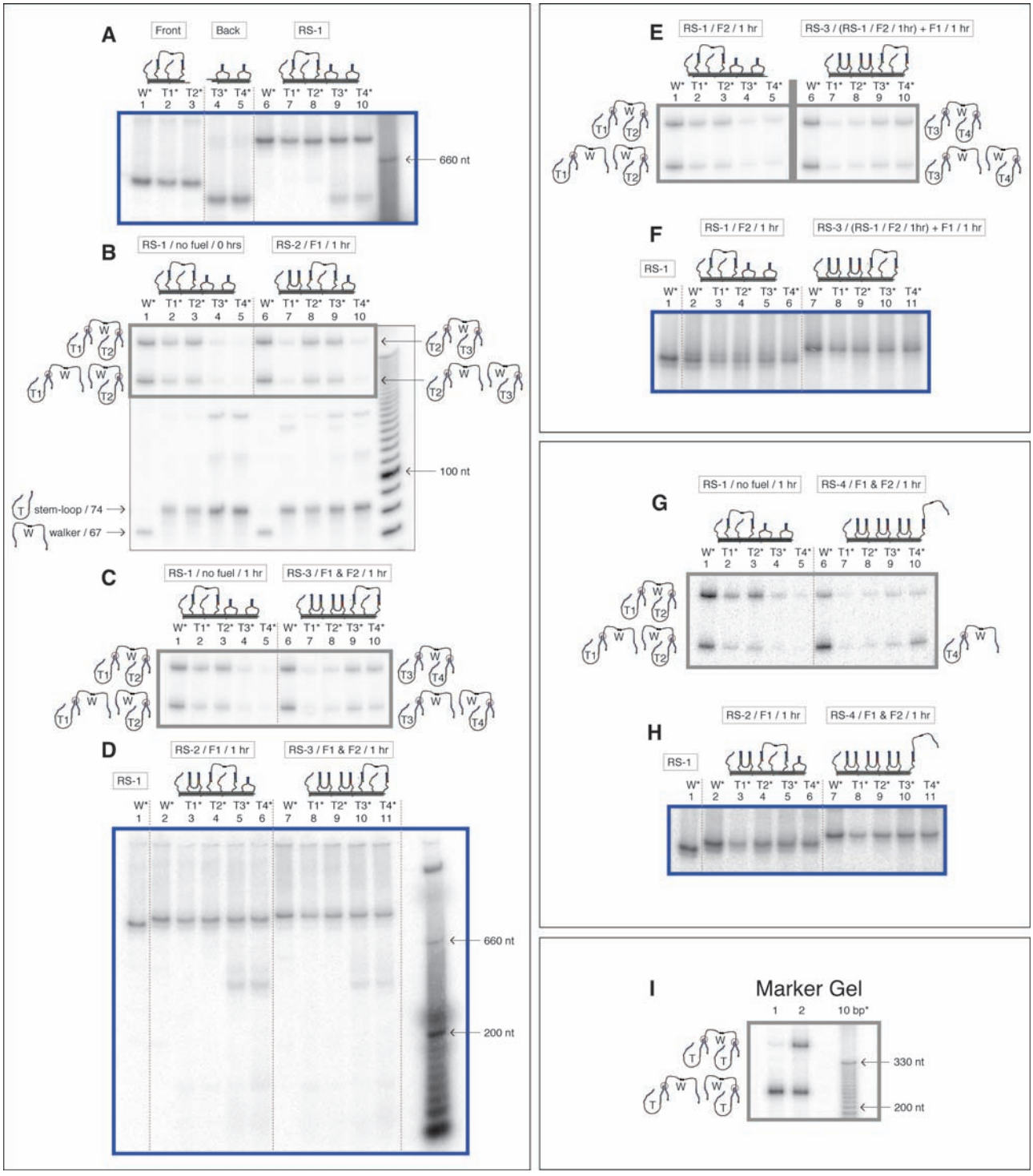

Fig. 4. Autoradiogram analysis of the walking cycle. Nondenaturing gels (all 4%) are outlined in blue, and super-denaturing gels (all 10%) are outlined in gray. Target products for the two states shown in each super-denaturing gel are drawn on the left and right hand side of each gel. (**A**) Nondenaturing gel verifying formation of the five radioactive tracks. (**B**) Super-denaturing gel showing the walker's position in RS-1 at 0 hours (lanes 1 to 5) and then in RS-2 (lanes 6 to 10) with the addition of F1 after 1 hour. (The box inside the gel outlines the walker–stem-loop cross-link products. See SOM text and figs. S8 to S11 for a detailed explanation of the secondary products seen on the super-denaturing gels as well as complete images of the super-denaturing gels.) (**C**) Super-denaturing gel verifying the transition to RS-3 (lanes 6 to 10) with the addition of F1 and F2 and no transition with no fuel added (lanes 1 to 5), both within an hour. (**D**) Nondenaturing gel verification of (B) and (C). (**E**) Composite super-denaturing gel showing the track remained in RS-1 while sitting in solution with F2 for 1 hour (lanes 1 to 5) and then transitioned to RS-3 when F1 was added to the mixture (lanes 6 to 10). [The gray line separates data from two different gels (fig. S10).] (**F**) Nondenaturing gel of (E). (**G**) Super-denaturing gel verifying the transition to RS-4 (lanes 6 to 10) with the addition of F1 and F2 and verification that the system remained in RS-1 (lanes 1 to 5) with no fuel added (lanes), both within an hour. (**H**) Nondenaturing gel verification of (G). (**I**) Marker gel showing the position of the w-t, w-l, and w-t-l products on a super-denaturing gel. (Complete pictures of the nondenaturing gels are outlined in the SOM text and fig. S12).

by track consumption. Hence, if given the choice between two directions, these walkers can go either way. In our system, directionality is a consequence of the asymmetry of the design, which is a key component of functional Brownian motors (*4*, *5*).

Through track stem-loop consumption, our mechanism allows the walker to hybridize the fuel hairpins onto the track sequentially and dynamically according to the presence of a code on the track. Such a capability in a molecular automaton is reminiscent of the ribosome and DNA or RNA polymerase (*26*). Indeed, the leg-holding sequences are uncoupled from the fuel-grabbing sequences. Thus, in principle, a track could be encoded to hybridize with an arbitrary number of fuel molecules before the walker returned to the beginning of the fuel cycle to take further steps in the same direction. This demonstration of molecular coordination is a step toward the development of more complex and autonomous synthetic molecular motor systems, whether they are made from DNA or from other polymeric materials (*5*).

References and Notes

1. K. Svoboda *et al.*, *Nature* **365**, 721 (1993).
2. A. D. Mehta, *Nature* **400**, 590 (1999).
3. R. D. Vale, *Cell* **112**, 467 (2003).
4. R. D. Astumian, *Science* **276**, 917 (1997).
5. E. R. Kay, D. A. Leigh, F. Zerbetto, *Angew. Chem. Int. Ed.* **46**, 72 (2007).
6. W. B. Sherman, N. C. Seeman, *Nano Lett.* **4**, 1203 (2004).
7. J. S. Shin, N. A. Pierce, *J. Am. Chem. Soc.* **126**, 10834 (2004).
8. Y. Tian, Y. He, Y. Chen, P. Yin, C. Mao, *Angew. Chem. Int. Ed.* **44**, 4355 (2005).
9. R. Pei *et al.*, *J. Am. Chem. Soc.* **128**, 12693 (2006).
10. P. Yin, H. M. T. Choi, C. R. Calvert, N. A. Pierce, *Nature* **451**, 318 (2008).
11. S. J. Green, J. Bath, A. J. Turberfield, *Phys. Rev. Lett.* **101**, 238101 (2008).
12. A. J. Turberfield *et al.*, *Phys. Rev. Lett.* **90**, 118102 (2003).
13. J. S. Bois *et al.*, *Nucleic Acids Res.* **33**, 4090 (2005).
14. T. J. Fu, N. C. Seeman, *Biochemistry* **32**, 3211 (1993).
15. P. Sa-Ardyen, A. V. Vologodskii, N. C. Seeman, *Biophys. J.* **84**, 3829 (2003).
16. B. Yurke, A. J. Turberfield, J. A. P. Mills, F. C. Simmel, J. L. Neumann, *Nature* **406**, 605 (2000).
17. J. B. Mills, E. Vacano, P. J. Hagerman, *J. Mol. Biol.* **285**, 245 (1999).
18. S. B. Smith, Y. J. Cui, C. Bustamante, *Science* **271**, 795 (1996).
19. S. G. Fischer, L. S. Lerman, *Cell* **16**, 191 (1979).
20. O. Gia, S. M. Magno, A. Garbesi, F. P. Colonna, M. Palumbo, *Biochemistry* **31**, 11818 (1992).
21. Material and methods are available as supporting material on *Science* Online.
22. T. J. Fu, Y. C. Tse-Dinh, N. C. Seeman, *J. Mol. Biol.* **236**, 91 (1994).
23. A 1-hour time interval was used in all of the experiments. This was an ideal time period for handling the five radioactive track versions simultaneously because all associated denaturing and nondenaturing experiments were conducted in parallel from one stock solution (*21*). Hence, detailed results about the reaction rates of the system are not available from this study.
24. J. Mai, I. M. Sokolov, A. Blumen, *Phys. Rev. E Stat. Nonlin. Soft Matter Phys.* **64**, 011102 (2001).
25. S. Saffarian *et al.*, *Science* **306**, 108 (2004).
26. E. Shapiro, Y. Benenson, *Sci. Am.* **294**, 44 (2006).

27. We thank C. Mao, H. Yan, and N. Jonoska for critical reading of the manuscript. This research has been supported by grants to N.C.S. from the National Institute of General Medical Sciences, NSF, the Army Research Office, the Office of Naval Research, the New York Nano-Bio-Molecular Information Technology Incubator program of the Department of Energy, and the W. M. Keck Foundation.

Supporting Online Material

www.sciencemag.org/cgi/content/full/324/5923/67/DC1
Materials and Methods
SOM Text
Figs. S1 to S14
Table S1
References

29 December 2008; accepted 10 February 2009
10.1126/science.1170336

Iron-Based Catalysts with Improved Oxygen Reduction Activity in Polymer Electrolyte Fuel Cells

Michel Lefèvre,* Eric Proietti,* Frédéric Jaouen, Jean-Pol Dodelet†

Iron-based catalysts for the oxygen-reduction reaction in polymer electrolyte membrane fuel cells have been poorly competitive with platinum catalysts, in part because they have a comparatively low number of active sites per unit volume. We produced microporous carbon–supported iron-based catalysts with active sites believed to contain iron cations coordinated by pyridinic nitrogen functionalities in the interstices of graphitic sheets within the micropores. We found that the greatest increase in site density was obtained when a mixture of carbon support, phenanthroline, and ferrous acetate was ball-milled and then pyrolyzed twice, first in argon, then in ammonia. The current density of a cathode made with the best iron-based electrocatalyst reported here can equal that of a platinum-based cathode with a loading of 0.4 milligram of platinum per square centimeter at a cell voltage of ≥0.9 volt.

The desired high power density from polymer electrolyte membrane fuel cells (PEMFCs) can only be achieved by speeding up the otherwise slow reaction steps at their low operating temperatures (~80°C) through catalysis. For the oxygen-reduction reaction (ORR), non–precious metal catalysts (NPMCs), which are potentially less expensive and more abundant, have been outperformed by Pt-based catalysts (*1*, *2*), which exhibit high activity as the native metal. For metals such as Co and Fe, improved performance will require a robust method for increasing the reactivity of the metal ion through ligation.

Since 1964, when Jasinski observed that cobalt phthalocyanine catalyzed the ORR (*3*), a number of approaches have been explored to create practical NPMCs. Catalysts were first obtained by adsorbing Fe-N_4 or Co-N_4 macrocycles on a carbon support and pyrolyzing the resulting material in an inert atmosphere (*4*). A breakthrough was then achieved by Yeager when it was revealed that these often-expensive macrocycles could instead be substituted by individual N and Co precursors (*5*). This approach was followed by several groups, including ours (*4*, *6*–*16*). Meanwhile, NPMC research using metal-N_4 macrocycles has also progressed (*17*–*19*).

Our previous approach in the synthesis of NPMCs for ORR has been to use NH_3 as a nitrogen precursor. The catalysts were obtained by wet impregnation of carbon black with an iron precursor such as iron(II) acetate (FeAc), followed by a heat treatment in NH_3; we refer to the products as Fe/N/C electrocatalysts. During pyrolysis at temperatures of ≥800°C, NH_3 partly gasifies the carbon support, resulting in a mass loss that depends on the duration of the heat treatment (*20*). The disordered domains of the carbon support are preferentially gasified (*21*–*23*). As a result, micropores are created in the carbon black particles. The mass loss at which maximum activity is reached [30 to 50 weight percent (wt %)] corresponds to the largest microporous surface area for the etched carbon, which suggests that these micropores (width ≤2 nm) host most of the catalytic sites (*21*).

The reaction of NH_3 with the disordered carbon domains also produces the N-bearing functionalities needed to bind iron cations to the carbon support (*24*, *25*). It has been proposed that most of the Fe/N/C catalytic sites consist of an iron cation coordinated by four pyridinic functionalities attached to the edges of two graphitic sheets, each belonging to adjacent crystallites on either side of a slit pore in the carbon support (*21*, *25*). Thus, four factors have been identified as requirements for producing active Fe-based catalysts for ORR: (i) disordered carbon content in the catalyst precursor (*20*), (ii) iron, (iii) surface nitrogen, and (iv) micropores in the catalyst.

Our present approach, which introduces a new material (pore filler) and replaces impregnation with planetary ball-milling, has elevated the catalytic activity of an Fe-based NPMC by a factor of >35 relative to the previous best reported

Institut National de la Recherche Scientifique, Énergie, Matériaux et Télécommunication, Varennes, Québec J3X 1S2, Canada.

*These authors contributed equally to this work.
†To whom correspondence should be addressed. E-mail: dodelet@emt.inrs.ca